Feasibility of a nitrogen-recombination soft-x-ray laser using capillary discharge *Z* pinch

N. S. Kampel, A. Rikanati, I. Be'ery, A. Ben-Kish, A. Fisher, and A. Ron
Department of Physics, Technion-Israel Institute of Technology, Haifa 32000, Israel
(Received 22 April 2008; published 17 November 2008)

Capillary discharge *Z* pinches have been shown to be efficient drivers for x-ray lasers (XRLs). In this work we examine the possibility of realizing a H_α nitrogen recombination laser ($3\rightarrow2$ transition) at $\lambda=13.4$ nm, using a capillary discharge *Z* pinch. A pulsed power generator with 60 kA peak current and 70 ns quarter period have been used to generate *Z*-pinch plasma in a 90-mm-long and 5-mm-diameter capillary. The plasma conditions were evaluated experimentally, using a filtered x-ray diode detector and time-integrated spectroscopy. The conditions required for the XRL were analytically estimated based on simple steady-state rate equations and then compared to experimental results. We demonstrated above 10% N^{7+} abundance at pinch time, while at least 50% is required. Then, in the expansion phase, the plasma is cooled in a time less than 5 ns to temperatures below 60 eV, as needed for the recombination laser. These results suggest that the required conditions for nitrogen-recombination lasing could be achieved in a capillary discharge *Z* pinch, but a higher-power driver might be needed.

DOI: 10.1103/PhysRevE.78.056404 PACS number(s): 51.50.+v, 52.25.−b, 52.30.−q

I. INTRODUCTION

Coherent soft-x-ray radiation can be used in a wide range of applications: high-resolution imaging and microscopy [1,2], lithography [2,3], time-of-flight spectroscopy with single-photon ionization [4], etc. There are several ways of realizing coherent soft-x-ray radiation: a soft-x-ray laser in highly ionized plasma [5,6], harmonic up-conversion of a high-power optical laser [7,8], synchrotron radiation [9], and the x-ray free electron laser (XFEL). In this paper we focus on achieving x-ray lasers (XRLs) by population inversion in multiply ionized ions.

There are primarily two different schemes for realizing XRLs, which differ in their pumping mechanisms. One scheme is based on collisional excitation in Ne-like or Ni-like ions [10]. This scheme was first demonstrated by Matthews *et al.* in 1985 at $\lambda\approx20$ nm ($3p\rightarrow3s$ transition of Ne-like selenium) [5]. The second scheme is based on three-body recombination in highly ionized plasma, as was first realized by Suckewer *et al.* in 1985 at $\lambda=18.2$ nm (H_α line of H-like carbon) [6].

In order to realize lasing in the three-body recombination scheme, there are two essential stages: plasma heating to the appropriate ionization level and then a fast enough cooling to escape thermal equilibrium. The nonequilibrium nature of the rapidly cooled plasma (faster then the three-body recombination rate) allows the three-body recombination of ions in the highest ionization level achieved in the heating phase to be dominant even at low temperatures. In such plasma, population inversion can be achieved (as will be further explained in the following sections) between the quantum level of the collision limit and the level below it. Slow cooling, through thermal equilibrium, will deplete the population of the highly ionized plasma, and high temperatures will eliminate the population inversion through thermal excitation to the lower lasing level. As can be understood, the difficulty in realizing three-body-recombination laser lies in achieving the rapidly cooled nonequilibrium plasma. The advantageous property of the recombination scheme is that the lasing occurs between two levels with different principal quantum numbers, $\Delta n=1$. The lasing transition energy is given by $\Delta E=R_yZ^2[n^{-2}-(n+1)^{-2}]$, where R_y is the Rydberg constant and *Z* is the ionization degree. Unlike the recombination scheme, in the collisional excitation scheme the laser transition is between two levels with different angular momentum $\Delta l=1$, with a transition energy of $\Delta E\cong2.7(Z-8)$ eV [10]. Therefore for a given ionization energy a shorter-wavelength laser can be obtained with the recombination scheme. This gives a strong motivation for implementing a high-gain-length recombination XRL.

To generate the highly ionized plasma needed for the XRL, there are two possible power drivers: high-power lasers [5,6,11,12], and electrical discharge *Z* pinch [13–16]. The use of capillary discharge *Z* pinch as a driver was first proposed for the recombination laser by Rocca *et al.* in 1988 [17]. In their system a high-current pulse ($I\gtrsim20$ kA) with a fast rise time ($dI/dt\gtrsim0.5$ kA/ns) flows through a carbon capillary and ablates the inner capillary wall, thus producing carbon plasma. The current through the plasma column produces an azimuthal magnetic field which compresses the plasma to the axis. At the pinch time (time of maximum compression), most of the plasma's kinetic energy thermalizes, producing a narrow column of hot dense plasma ($T_e\cong50$ eV and $N_e\cong5\times10^{18}\mathrm{cm}^{-3}$). In these experiments stimulated emission of the H_α line at $\lambda=18.2$ nm has been observed with a gain length up to 5 ($g\leqslant3\ \mathrm{cm}^{-1}$), but saturation was not achieved [16,18,19]. The major drawbacks in the ablative capillary discharge *Z*-pinch apparatus are a relatively short capillary ($\leqslant4$ cm), which limits the gain length, and low reproducibility [20]. These drawbacks originate from the high voltage needed for surface breakdown and the poor reproducibility of the surface breakdown in the carbon capillary.

Gas-filled capillary discharge *Z* pinches do not suffer from these drawbacks, and regularly produce long (up to 45 cm), narrow ($r_p\leqslant0.1r_0$), and stable plasma columns [14,15,21]. Capillary *Z*-pinch experiments have been used successfully for Ne-like argon and collisional excitation

XRL at $\lambda = 46.9$ nm [13,14], producing up to $E \approx 0.88$ mJ per pulse with 4 Hz repetition rate [21].

In this work we studied the theoretical and experimental requirements needed for the H-like nitrogen H_α recombination laser at $\lambda = 13.4$ nm, using a gas-filled capillary discharge Z pinch. The capillary discharge Z pinch apparatus has been shown to be capable of producing the required hot plasma conditions with a reasonable power driver. We also expect that the required cooling time period and cold plasma temperature can be realized through the hydrodynamic cooling generated by the rarefaction wave reflecting from the outer surface of the compressed plasma column moving toward the center. By simple estimations (which are beyond the scope of the current paper), other cooling mechanisms relevant to the Z-pinch process, such as heat conductance to the walls from the plasma column, were found to be negligible.

The main goal of this work is to compare experimental measurements on a fast ($dI/dt \cong 0.85$ kA/ns) capillary discharge Z-pinch plasma system to the required plasma conditions. Since the exact cooling time and final temperature achieved through the rarefaction wave cannot be easily modeled, fast diagnostics were implemented, focusing our measurements on the cooling stage.

Further support to our claim is shown in [22,23] through magnetohydrodynamic (MHD) calculations and gain estimations for our experimental apparatus, predicting maximum gain of 2 cm^{-1}. Since these calculations do not take into consideration all the physical effects, such as wall current, an experimental approach is needed to find the required pulsed power performance. In this paper we show that the required cooling time and the cold plasma temperature are appropriate for the recombination laser. On the other hand, the electron temperature at the pinch time (maximum temperature) is not sufficiently high to achieve the required fully stripped nitrogen abundance. In Sec. II we derive the required laser parameter and describe the Z-pinch dynamics. In Sec. III we describe the experimental apparatus and diagnostics. In Sec. IV we compare the required laser parameters (Sec. II) to our measurements.

II. THE REQUIRED PLASMA AND z-PINCH CONDITIONS

In the three-body recombination process $N_n^i + 2e \rightarrow N_m^{i-1} + e$, one electron is captured by the ion and a second electron gains the energy and momentum difference [10,24]. The rate of this process is proportional to $N_e^2 T_e^{-2}$ [10,24], where N_e is the electron density and T_e is the electron temperature. The captured electron is collisionally deexcited down to a specific level—the "collision limit." Levels above this limit are collisionally coupled to the continuum and levels below it are radiatively coupled to the ground state due to spontaneous decay (see Fig. 1). The collision limit is defined as the level for which the spontaneous decay rate is equal to the rate of collisional deexcitation into that level. As the electron temperature or density decreases, the collision limit increases.

The recombination laser is inherently a non-steady-state, time-dependent process. At the first stage the plasma is heated and the ions are highly ionized; then the plasma is cooled and the three-body recombination becomes the dominant process. At this stage electrons recombine and deexcite into the collision limit level (n_{lim}), while the lower laser level ($n_{\mathrm{lim}} - 1$) rapidly depletes due to spontaneous radiative decay. As a result, a population inversion occurs between n_{lim} and $n_{\mathrm{lim}} - 1$. Since we are interested in the H-like nitrogen-recombination laser, at least 50% of the ions should be fully stripped (N^{7+}) at the heating stage [10]. The relation between the ionization abundance and the electron temperature was calculated using a set of steady-state rate equations including collisional ionization, three-body recombination, and radiative recombination from the ground state [10,22]. This calculation indicates that an electron temperature above 140 eV is needed.

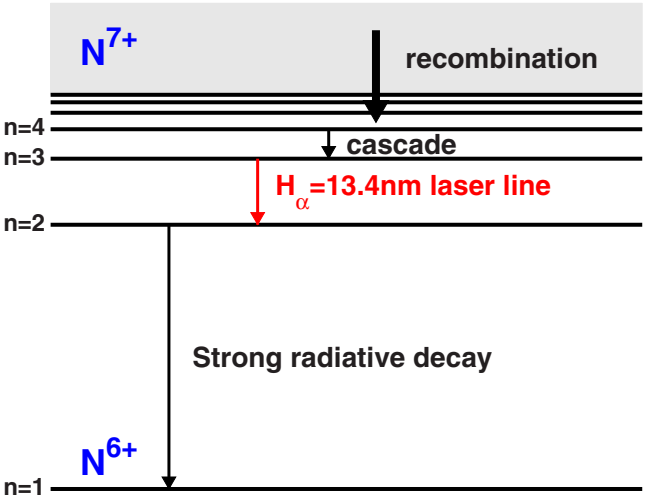

FIG. 1. (Color online) Simplified Grotrian diagram of H-like nitrogen showing the processes responsible for the generation of population inversion between the $n=3$ and $n=2$ levels in the 13.4 nm (H_α line) N^{6+} recombination laser.

For the required electron density there are two contradictory requirements. On the one hand, high electron density is needed for the dominance of the three-body recombination process. On the other hand, a low electron density and low electron temperature are needed to reduce collisional and resonant excitation into the lower lasing level ($n=2$), destroying the population inversion. The population inversion was estimated by examining the steady-state rate equation of the lower lasing level [10], and thus finding the ratio N_2/N_3. Equation (1) is the steady-state rate equation, which includes collisional excitation (X_{lu}), deexcitation X_{ul}, and spontaneous decay (A_{ul}), where l represents the lower level and u the upper level. The steady-state assumption is justified as long as the rate of depletion of the free electron reservoir and the rate of cooling are slow compared to the atomic processes time scale. In addition, optically thin plasma was assumed, i.e., negligible reabsorption. In [22] Varb *et al.* have calculated the nitrogen level dynamics, using MHD and the FLY atomic code. These calculations show negligible difference due to opacity. These results were also verified in our calculations using the FLY code.

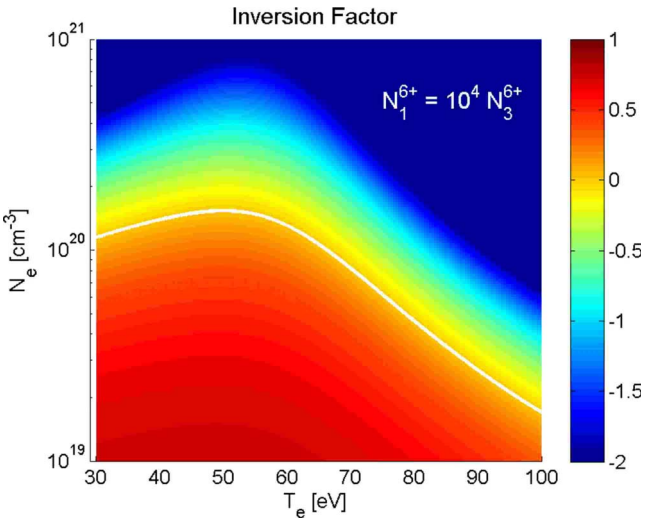

FIG. 2. (Color online) Inversion factor for various different electron densities and electron temperatures. The white line differentiates between a positive inversion factor (below it) and a negative inversion factor (above it). An $N_1=10^4N_3$ ratio was used to calculate the inversion factor.

$$\frac{dN_2}{dt} = 0 = N_3\left(N_eX_{32} + \frac{N_1}{N_3}N_eX_{12} + A_{32}\right) - N_2(N_eX_{23} + A_{21}). \tag{1}$$

In order to calculate the inversion factor using Eq. (2), we postulated a constant ratio between the populations of the upper lasing level and the ground state (N_1/N_3). This ratio represents how many of the ions are initially fully stripped, i.e., a higher ratio corresponds to a lower electron temperature at the pinch time. This is expected since as the electron temperature rise the abundance decreases and the ratio decreases. In [22,23] a ratio of 10^3 was calculated for an electron temperature of ~140 eV. Since the inversion factor decreases for higher N_1/N_3 ratio (lower electron temperature at the pinch time), we used the severe case of $N_1=10^4N_3$.

$$F \approx 1 - \frac{g_3}{g_2}\frac{N_eX_{32} + (N_1/N_3)N_eX_{12} + A_{32}}{N_eX_{23} + A_{21}}. \tag{2}$$

The inversion factor given in Eq. (2) was calculated for a wide range of electron densities and temperatures as shown in Fig. 2. The white line follows $F=0$, so a positive inversion factor corresponds to plasma conditions below that line. Figure 2 indicates that for positive gain the electron density should be below 10^{20} cm^{-3} and the electron temperature should be below 60 eV. At electron temperatures above 60 eV the collisional excitation from the ground state into the lower laser level will destroy the population inversion. These conclusions are almost independent of the ratio N_1/N_3 we postulated, but the absolute value of the gain does depend on this ratio.

The cooling rate should be fast enough not to deplete the population of totally stripped ions. Therefore the hydrodynamic cooling rate must be faster than the three-body-recombination rate, i.e., $\Delta t \lesssim R_{3BR}^{-1} \approx 5$ ns [12,25].

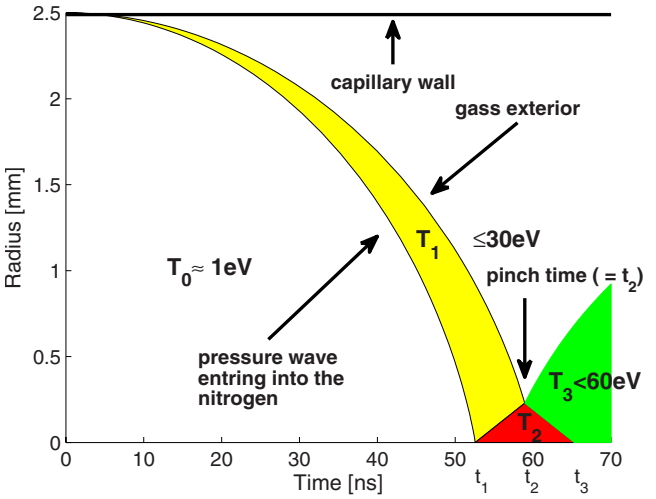

FIG. 3. (Color online) The pinch radius-time schematic map. Each color represents a different stage of the pinch and a different temperature.

In summary, the conditions required for the nitrogen-based recombination laser are that initially at least 50% of the ions should be fully stripped, which implies heating to electron temperatures above 140 eV. Then the plasma should be cooled to electron temperatures below 60 eV while maintaining electron densities of $(5-10)\times10^{19}$ cm^{-3} are maintained, and the cooling time should be less than 5 ns.

The dynamics of a z pinch is demonstrated in the radius-time schematics in Fig. 3. As the current rises in the capillary a pressure wave enters into the gas and compresses it. At this stage, which corresponds to $t<t_1$ and $T=T_1$ in Fig. 3, the plasma is not significantly heated, but accumulates kinetic energy. When the pressure wave reaches the center, $r=0$ and $t=t_1$ in Fig. 3, a shock wave is reflected, propagating outward (toward the capillary wall). The shock wave heats and ionizes the plasma to the temperature T_2 at times $t_1<t<t_3$. During $t_1<t<t_3$ the hot plasma emits x-ray radiation. Even though the maximum temperature is expected at t_1, maximum emission is expected when the shock wave leaves the plasma at $t=t_2$, since due to thermal conductivity the temperature in the triangle between t_1 and t_3 is only slightly lower than at t_1, while at t_2 a maximum volume of the hot plasma is achieved. The time of maximum compression and emission $(t=t_2)$ is also called the pinch time. When the shock wave leaves the plasma column, t_2 in Fig. 3, a rarefaction wave enters into the plasma, expanding it, and cooling it adiabatically to temperature T_3 (green area) in Fig. 3, within a time period t_3-t_2.

In this work we used a pulsed power generator with a peak current of $I_{max}=60$ kA and a quarter period of $\tau_{1/4}=70$ ns $(dI/dt\approx0.85$ kA/ns), (see right axis of Fig. 4). Ben-Kish *et al.* [14] used a pulsed power generator with a peak current of $I_{max}=40$ kA and a quarter period of $\tau_{1/4}=51$ ns $(dI/dt=0.78$ kA/ns) with an argon capillary discharge z pinch to obtain electron temperature of 100 eV and electron density of 10^{20}cm^{-3}. Therefore we expected that our current profile would be appropriate to achieve the desired electron temperature.

In addition to achieving the required electron temperature at the pinch time, a fast cooling is required $(\Delta t<5$ ns) for

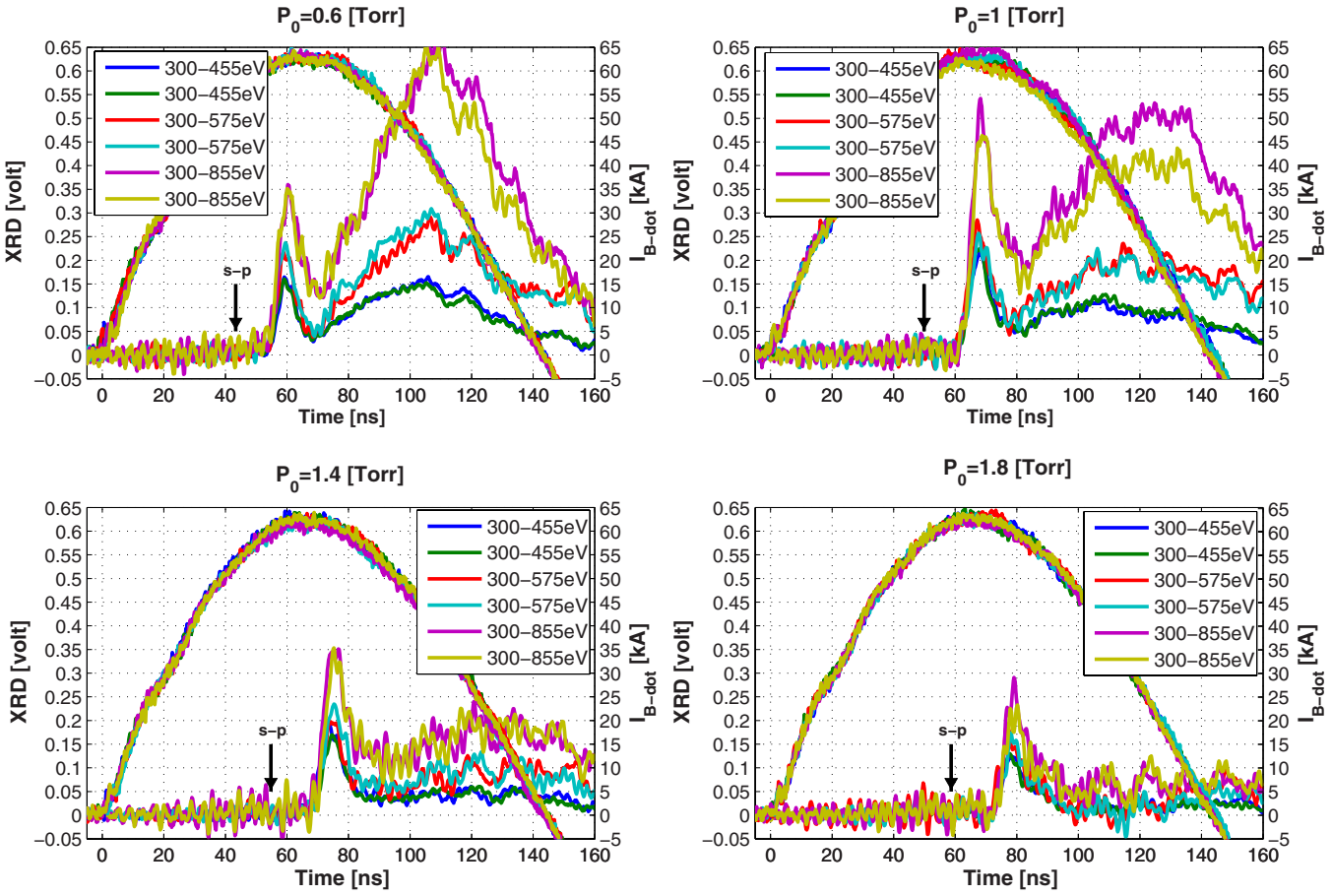

FIG. 4. (Color online) XRD signals (left axis) and current measurements (right axis) are shown as a function of the time. The legend shows the filter transmission energy (300–455 eV Ti, 300–575 eV Cr, and 300–855 eV Ni). Here we present four measurements with different initial pressures of N_2 molecules: 0.6 Torr, top left corner; 1 Torr, top right corner, 1.4 Torr, bottom left corner, and 1.8 Torr, bottom right corner. Good repeatability of the current and the XRD signals is evident.

the recombination laser. The total cooling time is estimated by the time it takes the rarefaction wave to traverse through the plasma column, i.e., $\Delta t_r = t_3 - t_2$ in Fig. 3, which depends on the rarefaction velocity (v_r) and the pinch radius (r_p). The rarefaction wave velocity is the sound velocity and was estimated in [26] to be $v_r \approx 10^7 \mathrm{cm\,s^{-1}}$. The pinch radius is usually less than one-tenth of the initial radius as was measured in [14]. Since we are using a 5-mm-diameter capillary, the expected total cooling time is estimated to be $t = r_p / v_r \approx 0.10 \times 0.25 / 10^7 = 2.5$ ns. We emphasize that the total cooling time is only an upper limit to the local cooling time at $r=0$, which is the time scale relevant for the lasing, i.e., a local cooling time of less then a few nanoseconds is expected.

Estimation of the gain achievable in our experimental system requires knowledge of the electron temperature and density profiles in order to calculate the atomic level abundance. Vrba *et al.* performed these calculation in [23], for the current profile and capillary radius of our system. They used a one-dimensional magnetohydrodynamic code (NPINCH) to calculate the temporal dynamics of the plasma electron temperature and density. Then they fed the hydrodynamic results into the FLY atomic code. These calculations predict gain up to $g = 2\mathrm{cm}^{-1}$ at initial nitrogen density of $N_0 = 1.4 \times 10^{17}\mathrm{cm}^{-3}$. Though these calculations predict gain, they do not take into consideration some important effects such as wall current. These effects might reduce the current that compresses the gas by up to 40% [27].

III. THE EXPERIMENTAL SETUP AND DIAGNOSTICS

A 5-mm-diameter and 90-mm-long quartz capillary discharge *Z*-pinch system has been built, with a pulsed power generator that produces a peak current of $I_{\max} = 60$ kA and a quarter period of $\tau_{1/4} = 70$ ns ($dI/dt = 0.85$ kA/ns). The current was measured using a $\tau = 2.1$ μs integrated detector, which measured the change in the magnetic flux. A fit of the measured current to an *RLC* circuit resulted in the following parameters: $R \approx 0.55$ Ω, $L \approx 165$ nH, $C = 12$ nF, $\tau_{1/2} \approx 140$ ns, and $V_0 = 280$ kV.

In a capillary discharge *Z* pinch, there is a problem of channel-like breakdowns. In gas-filled capillaries this problem is solved by using a prepulse [28], which ionizes the gas prior to the main pulse and ensures a uniform distribution of the main current (60 kA). The prepulse is a relative low current (40 A) passing through the capillary 2.5 μs before the main current pulse. In our case the prepulse also disassociates the N_2 molecules into two N atoms. Additionally, due to

the uniform plasma conditions achieved by the prepulse, the jitter in the *Z*-pinch process is smaller than 0.4 ns. This was measured by the emitted x-ray radiation (photon above 300 eV) as demonstrated in Fig. 4.

The characterization of the plasma was done using two different diagnostics: a time-resolved fast x-ray diode (XRD) with different filters and a time-integrated x-ray spectrometer. The filtered XRD measured the temporal dynamics of the plasma, and serves as a low-spectral-resolution spectrometer, since each filter transmits photons in a specific energy window. The combination of the time-integrated spectroscopy system with the known transmission of the filters has been used to infer which lines each filter transmits.

The XRD detector is based on the photoelectric effect. X-ray photons pass through a meshed anode, hitting the photocathode and releasing electrons. The photoelectrons accelerate to the anode due to a bias voltage (−500 V). We used a cesium iodide photocathode (evaporated on a nickel substrate), and measured the XRD rise time to be 0.3 ns with a response of 500 C/MJ. Due to the hygroscopic nature of the cesium iodide the response was one-third of the theoretical value, yet more than an order of magnitude higher than typically used materials such as polished carbon and gold with measured responses of 4 C/MJ, and 20 C/MJ, respectively.

The pinch emission was measured through on-axis and off-axis pinholes, using the XRD detector with different filters. In Fig. 4 the filtered XRD signals (left axis) and the current measurements (right axis) are shown for different shots. The measurements were taken for various initial gas pressures: 0.6, 1.0, 1.4, and 1.8 Torr of N_2 molecules. The reproducibility of these results implies very good stability of the plasma column, as expected from previous gas filled capillary discharge *Z*-pinch experiments [14,28].

The filtered XRD measures only photons with energy above 300 eV, therefore the signals correspond only to highly ionized ions. The XRD signal begins only when the inward-moving pressure wave reaches the capillary center (t_1 in Fig. 3) and an expanding shock wave is formed. The pinch time t_2 in Fig. 3 corresponds to the maximum emission time. For example, at initial gas pressure of 1.4 Torr the signal is zero until $t=70$ ns ($t<t_1$ in Fig. 3). At this time there is a fast rise of the signal for 3 ns, followed by a fast decay of the radiation for 5 ns. The pinch time is therefore $t_{\mathrm{pinch}}(1.4\ \mathrm{Torr})=73$ ns ($t=t_2$ in Fig. 3).

After the plasma has cooled from the shock, e.g., $t>70$ ns at initial pressure $P_0=0.6$ Torr, there remains substantial radiation for a relatively long time (tens of nanoseconds). The intensity of this radiation varies for the different filters and different initial density. The source of this radiation might be Ohmic heating, although it is not fully understood. The measured pinch time was compared to the predicted time of the snowplow model [29], shown as arrows in Fig. 4. As expected, the measured pinch time is 30–35 % (about 15 ns) longer than the snowplow prediction. This discrepancy is due to the simplifying assumptions of the model, mainly because it does not take into account effects such as wall current. Rituccci *et al.* [27] showed that about 30–40 % of the current flows in an ablative layer near the wall, which is consistent with our measurements.

A free standing, transmission grating, time-integrated spectroscopic system was built to infer which lines were

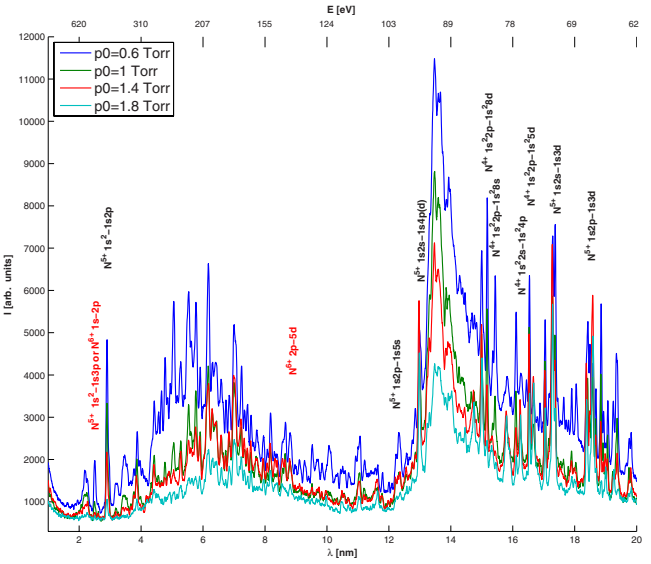

FIG. 5. (Color online) Time-integrated transmission grating spectroscopy results at four different initial gas densities, 0.6, 1.0, 1.4, and 1.8 Torr. Bottom *x* axis is the spectrum wavelength λ in nanometers. The Top *x* axis is the spectrum wavelength *E* in eV.

transmitted through each filter. The spectrometer system used a grating constant of $d=100$ nm with a linewidth of $S=35$ nm. A 100 μm slit was mounted in front of the grating, and the capillary emission was measured behind a 0.2-mm-diameter pinhole. The grating was located 316 mm from the capillary end, and 309.3 mm from the detector. A photostimulated luminescence (PSL) plate detector was used with a readout resolution of 17.5×17.5 $\mu\mathrm{m}^2$ per pixel. Since the capillary discharge *Z* pinch emits a low photon flux, we used the shortest possible distance between the capillary and the detector. Thanks to the reproducibility of the system, each measurement was an integration of ten consecutive shots. In general, as the distance between the plasma source and the detector increases, a better resolution is achieved [30]. Here, the resolving power is $\Delta\lambda/\lambda=20-200$ ($\Delta\lambda\approx0.13$ nm), and the wavelength range is 1.5–20 nm (the upper limit is due to the PSL plate width of 10 cm).

Figure 5 shows four measured spectra with different initial gas pressures. We observed the H-like nitrogen lines and the recombination spectra of H-like and fully stripped nitrogen. Observed lines that match published lines [31,32] to ~1 Å (the spectrometer resolution) are identified in Fig. 5. There are many lines that were not identified. These lines probably originate from the cathode and anode ablation at late times due to the time-integrated measurement. This ablation plasma, which consists of 70% tungsten and 30% copper, has many lines in the measured area, especially at $\lambda=3-10$ nm, where there are few nitrogen lines.

The spectrum can be divided into three different sections: $\lambda\geqslant11$ nm, $3\leqslant\lambda\leqslant11$ nm, and $\lambda\leqslant3$ nm. The spectrum at wavelengths above 11 nm consists mostly of Li-like nitrogen lines, from relatively cold plasma. This is expected in time-integrated measurements. The "broad" line observed at $\lambda=14\pm1$ nm is composed of Li-like, He-like, and H-like nitrogen lines.

Since there is no continuum radiation emitted at wavelengths above 9 nm (see Fig. 5) the measured spectrum at

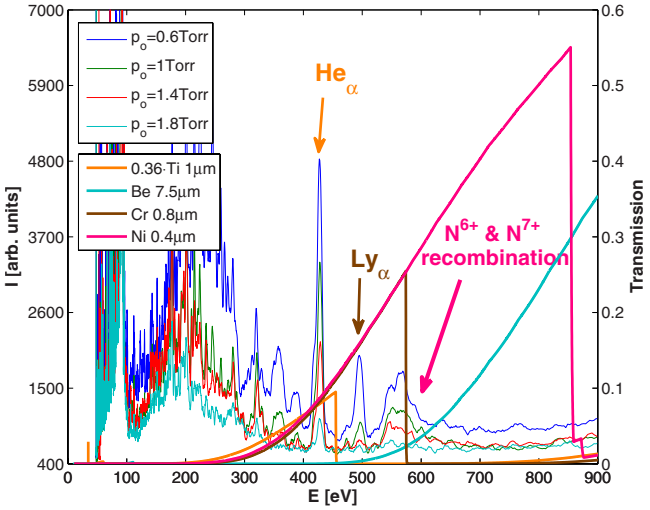

FIG. 6. (Color online) Filter transmission (right axis) and measured spectrum (left axis) as functions of photon energy.

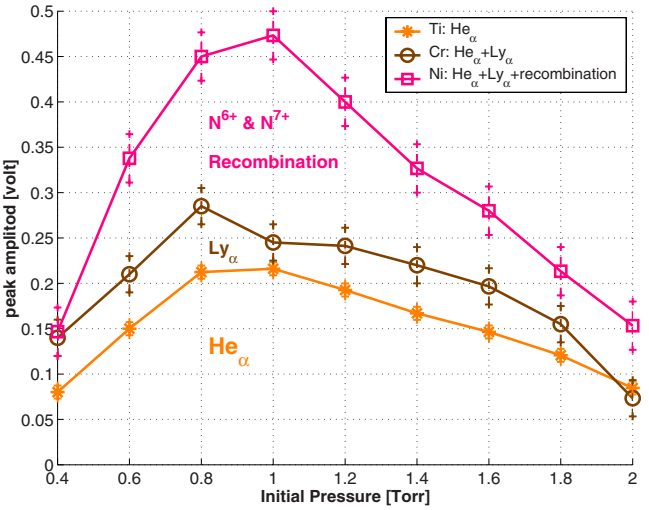

FIG. 7. (Color online) Peak XRD results as function of the initial gas pressure for the different filters. The contribution of the He-α line is shown as the orange (*) line, the Ly-α added contribution is shown between the brown (○) line and the orange (*) lines. The contribution of the recombination of H-like and fully stripped nitrogen is shown between the purple (□) and the brown (○) lines.

wavelengths 3–11 nm is not related to bremsstrahlung radiation. This spectrum corresponds to line emissions from the electrodes' ablated materials and to photorecombination of fully stripped nitrogen to H-like nitrogen at the second level ($n=2$, $\lambda=7.3$ nm). This is evident in the measurement at initial gas pressure of 0.6 Torr. In the measurements at higher initial gas pressure, there is also a contribution from recombination of H-like nitrogen to the second level of He-like nitrogen ($n=2$) with energy difference of about 130 eV ($\lambda=9.5$ nm).

The spectrum at wavelengths below 3 nm gives most of the information about the ionization abundance of the nitrogen plasma. In this region only nitrogen lines exist and accordingly the interpretation is straightforward. In these wavelengths, the filtered XRD signals were used to measure the ionization abundance dynamics, as well as to estimate the electron temperature. At-$\lambda=2.5$ nm ($E=500$ eV), there is an observable line, which is either the He-β line or the Ly-α line which cannot be distinguished with the resolution of our spectrometer.

We deduced that the observed line is mostly the Ly-α line, since its intensity increases as the initial pressure drops. A decrease of the initial pressure is expected to increase the electron temperature and to increase the abundance of H-like nitrogen [22,25].

The filters were chosen to transmit the He and the Ly series lines, i.e., photons originated from nitrogen ionized more than five times. Figure 6 shows the transmission of the filters (right axis) and the measured spectrum (left axis) as a function of the photon energy in eV. Comparison of the known filter transmission and the measured spectrum gives the transmitted spectrum for each filter. Here we used four different filters: 1 μm Ti filter that transmits the He-α line, 0.8 μm Cr filter that transmits the He-α line and the Ly-α line, and 0.4 μm Ni filter that transmits the He-α line, the Ly-α line with its satellites, and the recombination spectrum of H-like and fully stripped nitrogen. An extra filter that was used is a 7.5 μm Be filter, which transmits the recombination spectrum of the H-like and fully stripped nitrogen.

IV. COMPARISON OF THE REQUIRED LASER CONDITIONS TO THE MEASURED PLASMA CONDITIONS

The Z-pinch conditions are inferred by using the filtered XRD signals and their interpretation using time-integrated spectroscopy. The peak amplitude of the XRD signal as a function of initial gas pressure, given in Fig. 7, indicates the intensity of the different lines at the pinch time. The contribution of the He-α line is given by the orange (*) line in Fig. 7. The added contribution of the Ly-α line is the difference between the brown (○) and the orange (*) lines. The contribution from the recombination of H-like and fully stripped nitrogen is given by the difference between the purple (□)

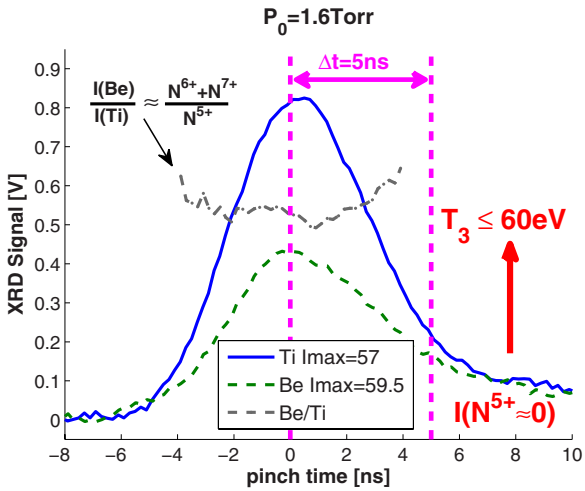

FIG. 8. (Color online) Zoom on the pinch time of the XRD signals using the Ti (solid line) and Be (dashed line) filters as function of time. In black (dot-dashed line) is shown the ratio between the XRD signal with the Be filter and the Ti signal.

and brown (○) lines. These relative radiation intensities give an indication of the ionization abundance. From Fig. 7 it is evident that there is a significant contribution of the H-like and fully stripped nitrogen-recombination radiation. For example, at initial gas pressure of 1 Torr the contribution from recombination radiation of H-like and fully stripped nitrogen is twice the emitted radiation from the He-α and Ly-α lines. Therefore we estimate that the ionization abundance of fully stripped nitrogen at the pinch time is above 10%. This relative ionization abundance corresponds to electron temperatures higher than 100 eV, in local thermal equilibrium approximation [22].

The required electron density for the laser is $(5-10)\times 10^{19}$ cm^{-3}. The ion density of the Z pinch at maximum compression is estimated from the initial gas density and the compression ratio. The electron density is then the ion density times the average ionization. Equation (3) gives the electron density as a function of the initial gas density. To reach the necessary electron density at the pinch time, the initial gas density should be $N_0 \approx 7\times 10^{16}$ cm^{-3}, which is equivalent to initial pressure $P_0 \approx 1$ Torr of N_2 molecules.

$$N_e = zN_i = z\left(\frac{R_0}{R_p}\right)^2 N_0 \approx 10^3 N_0. \tag{3}$$

The temporal dynamics of the pinch is demonstrated using the XRD signals with the Ti and Be filters. These XRD signals at initial gas pressure of 1.6 Torr are shown in Fig. 8. The period $t<-5$ ns in Fig. 8 corresponds to the time before the shock wave is formed ($t<t_1$ in Fig. 3). At this stage we do not measure any radiation of He-like nitrogen. Based on the steady-state rate equation [22], the electron temperature is estimated to be less than 30 eV (T_1 in Fig. 3).

When the shock wave is formed at the center and expands ($t_1<t<t_2$ in Fig. 3), the plasma significantly heats up and ionizes. At this time the XRD signal starts to rise ($t>-5$ ns in Fig. 8) due to emission from He-like, H-like, and fully stripped nitrogen. The maximum emission is measured at the pinch time $t=0$ ns (t_2 in Fig. 3). When the shock wave leaves the plasma column, a rarefaction wave enters the plasma and lowers its temperature. As the rarefaction wave traverses toward the plasma center, the emission from He-like nitrogen drops. After 5 ns the rarefaction wave reaches the center and the XRD signal almost vanishes completely (t_3 in Fig. 3). Therefore the total cooling time of the plasma is less than 5 ns. Additionally, since the emission from He-like nitrogen is negligible after the rarefaction, the plasma temperature is less than 60 eV, i.e., $T_3<60$ eV in Fig. 3. We emphasize again that the total cooling time, measured using the XRD, is only an upper limit for the local cooling time at $r=0$, which is expected to be much faster. The ratio between the filtered XRD signals (Be to Ti) throughout the pinch (± 4 ns in Fig. 8) is constant and time independent for all initial gas pressures, as is demonstrated in Fig. 8 (black dot-dashed line). Therefore, for the duration of the pinch, the ion abundance ratio does not change significantly, i.e., $(N^{6+}+N^{7+})/N^{5+} \approx$ const. This could be understood if the temperature of the shocked plasma is almost constant ($T_2 \approx$ const in Fig. 3), while the preshock and postrarefaction plasma is much colder and does not contribute significantly to the XRD signals.

TABLE I. Comparison between the needed conditions for the nitrogen recombination XRL and the measured z-pinch plasma condition.

	Condition	Requirement	Demonstrated
1	N^{7+} abundance	$\sim 50\%$	$>10-20\,\%$
	Pinch T_e	~ 140 eV	$\geqslant 100$ eV
2	N_e density	$(5-10)\times 10^{19}$ cm^{-3}	$\approx(5-10)\times 10^{19}$ cm^{-3}
3	Final T_e	$T_e \leqslant 60$ eV	$T_e \leqslant 60$ eV
4	Cooling duration	$\Delta t \leqslant 5$ ns	$\Delta t \leqslant 5$ ns

V. SUMMARY

The capillary discharge Z-pinch plasma has been considered as a driver for a nitrogen-based recombination XRL with the H_α line ($3\rightarrow 2$ transition). In this work we compared the plasma conditions require for a recombination laser with the plasma obtained using a capillary discharge Z pinch. The experimental setup consisted of a 5-mm-diameter and 90-mm-long quartz capillary and a pulse power generator with a peak current of $I_{\max} \cong 62$ kA and a quarter time period of $\tau_{1/4}=70$ ns ($dI/dt \cong 0.85$ kA/ns). The plasma conditions were examined using two diagnostics. A 0.3 ns rise time XRD with appropriate filters served as a time-dependent low-resolution spectrometer. The second diagnostic was a 1 Å resolution, free standing transmission grating spectrometer coupled to a photo stimulated luminescence plate, which gave a time-integrated spectrum.

These diagnostics were used to estimate the plasma conditions at different stages of the z pinch. Table I summarizes the required plasma conditions and the evaluated experimental plasma conditions. The results show that all the needed conditions for nitrogen recombination laser are realized in the capillary discharge Z-pinch system, with the possible exception of low N^{7+} abundance. It is speculated that a more powerful power generator with a similar rise time could reach the goal of at least 50% fully stripped nitrogen, and significant lasing.

ACKNOWLEDGMENTS

We gratefully acknowledge the technical assistance of Uri Avni, Zvi Shwimmer, Igal Levi, and Yoav Erlich in building and designing the experimental apparatus and performing the experiments. This work was partially supported by the Fund for Encouragement of Research at the Technion.

[1] G. Vaschenko *et al.*, Opt. Lett. **31**, 1214 (2006).
[2] A. Ritucci, A. Reale, P. Zuppella, L. Reale, P. Tucceri, G. Tomassetti, P. Bettotti, and L. Pavesi, J. Appl. Phys. **102**, 034313 (2007).
[3] V. Banine and R. Moors, J. Phys. D **37**, 3207 (2004).
[4] S. Heinbuch, F. Dong, J. J. Rocca, and E. R. Bernstein, J. Chem. Phys. **126**, 244301 (2007).
[5] D. L. Matthews *et al.*, Phys. Rev. Lett. **54**, 110 (1985).
[6] S. Suckewer, C. H. Skinner, H. Milchberg, C. Keane, and D. Voorhees, Phys. Rev. Lett. **55**, 1753 (1985).
[7] Z. Chang, A. Rundquist, H. Wang, M. M. Murnane, and H. C. Kapteyn, Phys. Rev. Lett. **79**, 2967 (1997).
[8] T. Ditmire, J. K. Crane, H. Nguyen, L. B. DaSilva, and M. D. Perry, Phys. Rev. A **51**, R902 (1995).
[9] D. Attwood, K. Halbach, and K. Kim, Science **228**, 1265 (1985).
[10] R. C. Elton, *X-Ray Lasers* (Academic, New York, 1990).
[11] K. A. Janulewicz, J. Tümmler, G. Priebe, and P. V. Nickles, Phys. Rev. A **72**, 043825 (2005).
[12] D. Korobkin, A. Goltsov, A. Morozov, and S. Suckewer, Phys. Rev. Lett. **81**, 1607 (1998).
[13] J. J. Rocca, V. Shlyaptsev, F. G. Tomasel, O. D. Cortázar, D. Hartshorn, and J. L. A. Chilla, Phys. Rev. Lett. **73**, 2192 (1994).
[14] A. Ben-Kish, M. Shuker, R. A. Nemirovsky, A. Fisher, A. Ron, and J. L. Schwob, Phys. Rev. Lett. **87**, 015002 (2001).
[15] G. Tomassetti *et al.*, Opt. Commun. **231**, 403 (2004).
[16] C. Steden and H. J. Kunze, Phys. Lett. A **151**, 534 (1990).
[17] J. J. Rocca, D. C. Beethe, and M. C. Marconi, Opt. Lett. **13**, 565 (1988).
[18] H. J. Shin, D. E. Kim, and T. N. Lee, Phys. Rev. E **50**, 1376 (1994).
[19] R. Dussart, W. Rosenfeld, N. Richard, D. Hong, C. Cachoncinlle, C. Fleurier, and J. M. Pouvesle, in *Proceedings of the sixth International Conference on X-Ray Lasers*, edited by Y. Kato, H. Takuma, and H. Daido, (Institute of Physics and Physical Society, London, 1998), p. 171.
[20] J. J. Rocca and M. C. Marconi (private communication).
[21] C. D. Macchietto, B. R. Benware, and J. J. Rocca, Opt. Lett. **24**, 1115 (1999).
[22] P. Vrba, M. Vrbova, N. A. Bobrova, and P. V. Sasorov, Cent. Eur. J. Phys. **3**, 564 (2005).
[23] P. Vrba and M. Vrbova, Czech. J. Phys. **56**, B425 (2006).
[24] H. R. Griem, *Plasma Spectroscopy* (McGraw-Hill, New York, 1964).
[25] K. Lee, J. H. Kim, and D. Kim, Phys. Plasmas **9**, 4749 (2002).
[26] C. H. Nam, E. Valeo, and S. Suckewer, J. Opt. Soc. Am. B **3**, 1199 (1986).
[27] A. Ritucci *et al.*, Contrib. Plasma Phys. **43**, 88 (2003).
[28] M. Shuker, A. Ben-kish, R. A. Nemirovsky, A. Fisher, and A. Ron, Phys. Plasmas **13**, 013102 (2006).
[29] D. D. Ryutov, M. S. Derzon, and M. K. Matzen, Rev. Mod. Phys. **72**, 167 (2000).
[30] S. Sailaja, V. Arora, S. R. Kumbhare, P. A. Naik, P. D. Gupta, D. A. Fedin, A. A. Rupasov, and A. S. Shikanov, Meas. Sci. Technol. **9**, 1462 (1998).
[31] R. L. Kelly, *Atomic and Ionic Spectrum Lines below 2000 Angstroms: Hydrogen through Krypton, Part I (H-Cr)* (American Chemical Society, New York, 1987), Vol. 16.
[32] http://physics.nist.gov/PhysRefData